

# Far-Infrared OH fluorescent emission in Sagittarius B2<sup>1</sup>

Javier R. Goicoechea and José Cernicharo<sup>2</sup>

*Instituto de Estructura de la Materia. Departamento Física Molecular, CSIC, Serrano 121,  
E-28006 Madrid, Spain.*

javier@isis.iem.csic.es

cerni@astro.iem.csic.es

## ABSTRACT

We present Infrared Space Observatory (ISO) observations of <sup>16</sup>OH and <sup>18</sup>OH toward Sgr B2 with a spectral resolution of  $\sim 35$  km s<sup>-1</sup>. The OH J=5/2→3/2 and J=3/2→1/2 rotational lines of the <sup>2</sup>Π<sub>1/2</sub> ladder are seen in emission while the cross-ladder transitions (from the <sup>2</sup>Π<sub>3/2</sub> J=3/2 to the J=1/2, 3/2 and 5/2 levels of the <sup>2</sup>Π<sub>1/2</sub> ladder), and the <sup>2</sup>Π<sub>3/2</sub> J=5/2←3/2 and J=7/2←5/2 lines are detected in absorption. The <sup>18</sup>OH <sup>2</sup>Π<sub>3/2</sub> J=5/2←3/2 Λ-doublet at  $\sim 120$  μm is also observed in absorption. All OH Λ-doublets are resolved (except the  $\sim 98$  μm) and show, in addition to the strong absorption at the velocity of Sgr B2, several velocity components associated to the gas surrounding Sgr B2 and to the foreground clouds along the line of sight.

No asymmetries in the line intensities of each doublet have been observed. We have modeled the observations using a non-local radiative transfer code and found that the OH absorption/emission must arise in a shell around Sgr B2 not resolved by the ISO/LWS beam. The gas density is moderate, with upper limits of 10<sup>4</sup> cm<sup>-3</sup> and  $\simeq 300$  K in temperature. The OH abundance is high,  $(2-5) \times 10^{-6}$ . We argue that a widespread photon dominated region explains the enhancement of OH abundance.

*Subject headings:* infrared: ISM: lines and bands — ISM: individual (Sgr B2)  
— ISM: molecules — line: identification — molecular data — radiative transfer

---

<sup>1</sup>Based on observations with ISO, an ESA project with instruments funded by ESA Member States (especially the PI countries: France, Germany, the Netherlands and the United Kingdom) and with participation of ISAS and NASA.

<sup>2</sup>Visiting Scientist, Division of Physics, Mathematics and Astronomy, California Institute of Technology, MS 320-47, Pasadena, CA 91125, USA

## 1. Introduction

The Sagittarius B2 complex represents an interesting burst of massive star formation in the Galactic Center (GC) and may be representative of other active galactic nuclei. Large scale continuum maps from radio to far-IR wavelengths show that Sgr B2 is the brightest and among the most massive clouds of the GC (Cox & Laureijs 1989, Pierce-Price et al. 2000; Scoville, Solomon & Penzias 1975). The Sgr B2 M source is the brightest far-IR condensation of the complex with a diameter of  $\simeq 40''$  at  $100\ \mu\text{m}$  (Goldsmith et al. 1992) and has also the largest gas column density (Lis & Goldsmith 1989). These studies have shown that the core is embedded in an extended and clumpy cloud of warm gas. However, the observed rich chemistry in the gas in front of Sgr B2 and its possible heating mechanisms are far from settled. Low velocity shocks have been invoked to explain the enhanced abundances of some species such as  $\text{NH}_2$  or  $\text{NH}_3$  (Flower, Pineau des Forêts & Walmsley 1995) which are not observed in more quiescent regions. On the other hand, UV radiation can have an important effect on the gas in the outer layers. This radiation may be provided by evolved stars and by young massive stars in the envelope of Sgr B2 itself (Martín-Pintado et al. 1999). In addition, the emission of several ions with high excitation potential (such as [OIII] and [NIII]) is extended in the Sgr B2 region (Goicoechea et al. 2003, in preparation). Thus, a widespread ionized component producing photodissociation regions (PDRs) in the envelope is also possible. In any of these scenarios or in a combination of both, O-bearing species such as  $\text{H}_2\text{O}$ ,  $\text{OH}$ ,  $\text{H}_3\text{O}^+$  and atomic oxygen are decisive for the thermal balance of the dense molecular gas (Neufeld et al. 1995). In particular, the hydroxyl radical,  $\text{OH}$ , has been predicted to be abundant in both scenarios.

The structure of the  $\text{OH}$  levels is depicted in Figure 1. The fundamental rotational  $\Lambda$ -doublet ( $\sim 119\ \mu\text{m}$ ) was first detected in the direction of Sgr B2 in absorption against the thermal dust emission by Storey, Watson & Townes (1981). Each line of the doublet is so optically thick that absorbs completely the continuum radiation avoiding any check with the models. These lines are detected over a large area ( $9' \times 27'$ ) around Sgr B2 (Cernicharo et al. 1999). A detailed study of the far-IR spectrum of  $\text{OH}$  has been carried out mainly in the Orion shocked region (Watson et al. 1985; Viscuso et al. 1985; Melnick et al. 1987, 1990; Betz & Boreiko 1989) but little is known toward GC clouds such as the gas in the line of sight toward Sgr B2.

From the theoretical point of view, Offer & van Dishoeck (1992; hereafter OfD) and Offer, van Hemert & van Dishoeck (1994; hereafter OfHD) have made detailed calculations of the collisional cross sections between  $\text{OH}$  and  $\text{H}_2$  and of the expected intensity of the  $\text{OH}$  far-IR lines. They predicted strong asymmetries in the intensity of the  $\text{OH}$   $\Lambda$ -doublets due to important asymmetries in the collisional rates between  $\text{OH}$  and para- $\text{H}_2$ .

In this letter, we present high-resolution observations of several OH  $\Lambda$ -doublets toward Sgr B2 involving levels up to  $\sim 420$  K. All lines inside the  $^2\Pi_{1/2}$  ladder are seen in emission while all the remaining lines are detected in absorption. The data have been modeled using a non-local radiative transfer code in order to constrain some important physical parameters of the warm outer layers of Sgr B2 and of the foreground gas.

## 2. Observations, Data Reduction and Results

Most of the pure rotational lines of OH are in the far-IR wavelength coverage of the Long-Wavelength Spectrometer (LWS; Clegg et al. 1996) on board ISO (Kessler et al. 1996). The ISO data base observations used in this Letter are 32201429, 32600502, 46201118, 46201123, 46701803, 47600809, 47608099, 49401705, 50400823, 50601013, 50600603, 50700610, and 84500102. The LWS/Fabry-Perot (FP) spectral resolution is  $\simeq 0.015 \mu\text{m}$  ( $\sim 35 \text{ km s}^{-1}$ ) and allows resolving the  $\Lambda$ -doubling of OH and its isotopes. Several OH rotational lines (intra and cross-ladder) were searched toward Sgr B2 M. Data are shown in Figure 1. The OH  $J=5/2 \leftarrow 3/2$  cross-ladder doublet at  $\sim 34 \mu\text{m}$  was observed with the Short-Wavelength Spectrometer (SWS; de Graauw et al. 1996) with a spectral resolution of 1500 (ISO observation 28702002). One component was observed with the SWS/FP with a velocity resolution of  $\sim 10 \text{ km s}^{-1}$  (ISO observation 46001217). When compared to the grating observation, the mean LWS/FP continuum flux of each line deviates by at least 20%, similar to the grating flux calibration errors (Swinyard et al. 1998). The systematic uncertainties are always larger than the statistical errors associated with the line signal-to-noise ratios (S/N). The best calibration is obtained by correcting the continuum level of the FP spectrum in order to coincide with the grating level. A polynomial baseline was fitted to each spectra and adopted as the continuum level. The effective SWS/FP aperture in the  $\sim 34 \mu\text{m}$  range is  $17'' \times 40''$ , while the LWS aperture is circular and  $\sim 80''$  in diameter. All the SWS and LWS products were processed with version 10.1 of the pipeline and analyzed using the ISO spectrometers data reduction package ISAP.<sup>3</sup>

Sgr B2 M has been the target of several spectroscopic observations in the far-IR. Molecular features have been always found in absorption. However, OH shows a different behavior. All rotational doublets connecting the  $^{16}\text{OH } ^2\Pi_{3/2}$  ground-state with the rotational levels of the  $^2\Pi_{1/2}$  ladder ( $\sim 34, 53, 79$  and  $119 \mu\text{m}$ ) are observed in absorption while the  $^{16}\text{OH } ^2\Pi_{1/2}$  intra-ladder rotational transitions at  $\sim 98$  and  $\sim 163 \mu\text{m}$  are observed in emission.

---

<sup>3</sup>The ISO Spectral Analysis Package (ISAP) is a joint development by the LWS and SWS Instruments Teams and Data Centers. Contributing institutes are CESR, IAS, IPAC, MPE, RAL, and SRON.

The  $\sim 79$  and  $\sim 53$   $\mu\text{m}$   $\Lambda$ -doublets have maximum absorption depths at the velocity of Sgr B2 M ( $V_{LSR} \simeq +50$   $\text{km s}^{-1}$ ). Nevertheless, there is still a contribution from more negative velocity components associated with the “spiral arms clouds” in the line of sight and with the gas surrounding the GC, which we divide in two components ( $\simeq -85$  and  $0$   $\text{km s}^{-1}$ ). The  $n(\text{H}_2)$  range found in these clouds varies from  $10^2$  to  $10^4$   $\text{cm}^{-3}$  (Greaves 1995). The absorption depths at  $V_{LSR} \simeq -85$   $\text{km s}^{-1}$  are  $\simeq 30\%$  and  $\simeq 15\%$  for the  $\sim 79$  and  $\sim 53$   $\mu\text{m}$  doublets respectively. These components are thought to arise in the molecular gas within 1 kpc of the GC (Scoville 1972). Assuming that the absorption at these velocities is optically thin and considering only radiative excitation (i.e., low  $T_{ex}$ ), we derive  $\chi(\text{OH}) \sim 10^{-6}$  for  $N(\text{H}_2) \simeq (5-10) \times 10^{21}$   $\text{cm}^{-2}$  (see Neufeld et al. 2000 for a distribution of  $N(\text{H}_2)$  in the line of sight). The opacity of the OH lines at  $V_{LSR} \simeq 0$   $\text{km s}^{-1}$  allows also to derive  $\chi(\text{OH}) \sim 5 \times 10^{-7}$  for  $N(\text{H}_2) \simeq 2.5 \times 10^{22}$   $\text{cm}^{-2}$ . This component is believed to arise in the diffuse gas at galactocentric radii 3–8 kpc and in the Solar vicinity (Greaves & Williams 1994). These values are higher than the typical OH abundances of  $10^{-7}$  found in diffuse and translucent clouds (Van Dishoeck & Black 1986).

The  $\sim 84$   $\mu\text{m}$  doublet and the  $34.603$   $\mu\text{m}$  line component (in absorption) and the  $^2\Pi_{1/2}$  doublets at  $\sim 98$  and  $\sim 163$   $\mu\text{m}$  (in emission) are strictly centered at the velocity of Sgr B2 M and are decisive to understand the excitation scheme of the molecule. The ISO data also provide upper limits to the emission/absorption of the  $J=3/2 \rightarrow 5/2$  ( $\sim 96$   $\mu\text{m}$ ) and  $J=5/2 \rightarrow 5/2$  ( $\sim 48$   $\mu\text{m}$ ) cross-ladder transitions and to the  $^2\Pi_{3/2}$   $J=9/2 \rightarrow 7/2$  ( $\sim 65$   $\mu\text{m}$ ) and  $^2\Pi_{1/2}$   $J=7/2 \rightarrow 5/2$  ( $\sim 71$   $\mu\text{m}$ )  $\Lambda$ -doublets of 1.5% of the continuum emission. Finally, we present the detection of the fundamental  $^{18}\text{OH}$   $^2\Pi_{3/2}$   $J=5/2 \leftarrow 3/2$  lines at  $\sim 120$   $\mu\text{m}$ . Apart from the feature associated with Sgr B2, there is another absorption at  $V_{LSR} \simeq 0$   $\text{km s}^{-1}$ . The derived  $^{18}\text{OH}$  column density is  $(2.5 \pm 0.5) \times 10^{13}$   $\text{cm}^{-2}$ , implying an  $^{16}\text{OH}/^{18}\text{OH}$  abundance ratio in this component of  $\sim 500$ , similar to the terrestrial value.

### 3. Modeling Sgr B2 and Discussion

The typical OH abundance in dense quiescent clouds is  $(0.1-1) \times 10^{-7}$  with OH/ $\text{H}_2\text{O}$  ratios in the range 1 to  $10^{-2}$  (Bergin et al. 1995). According to the chemical models, the major contribution to the enhanced OH abundance comes from regions where water vapor is being rapidly photodissociated (Sternberg & Dalgarno 1995) or regions in which shock waves play a role (Draine et al. 1983). In the case of Sgr B2, the innermost regions of the cloud are completely hidden in the mid and far-infrared due to the large dust opacity. Almost all the observed far-IR OH come from the external layers of the Sgr B2 cloud, i.e., from the surrounding gas at high  $T_K$  and from the cold dark clouds and diffuse gas in the line of sight.

In order to estimate the OH abundance and the physical conditions leading to the observed OH line emission in the  $V_{LSR} \simeq +50 \text{ km s}^{-1}$  component, we have modeled the first 20 OH rotational levels using the code developed by González-Alfonso & Cernicharo (1993). The hyperfine structure of OH is not included in the model. The collisional cross sections of OfHD have been used (kindly provided in electronic form by E.F van Dishoeck). We have adopted a spherical geometry for a cloud consisting of two components: a uniform core with a diameter of  $25''$  ( $3.2 \times 10^{18} \text{ cm}$  for an assumed distance to Sgr B2 of 8.5 kpc), with a dust temperature of 30 K (see Goicoechea & Cernicharo, 2001) and opacity at  $80 \mu\text{m}$  of 5 ( $\tau_\lambda = \tau_{80} * (80/\lambda(\mu\text{m}))$ ), and a shell of variable thickness and distance to the core. The shell was divided into 14 layers. All molecular transitions in the core are thermalized to the dust temperature due to the large dust opacity in the far-IR. In order to check the sensitivity of the results on the physical parameters,  $n(\text{H}_2)$ ,  $T_K$  and  $N(\text{OH})$  were varied from  $10^3$  to  $10^5 \text{ cm}^{-3}$ , 40 to 600 K, and  $1 \times 10^{15}$  up to  $1 \times 10^{17} \text{ cm}^{-2}$  respectively.

The observations put some constraints on the size and density of the shell. Excitation temperatures for the cross-ladder and  $^2\Pi_{3/2}$  transitions have to be below the dust temperature in order to reproduce the observed line absorptions. In addition, the shell thickness and its distance to the core cannot be large compared to the core size, otherwise limb effects introduce important re-emission that could cancel the absorption produced by the gas in front of the core. The results for some models are reproduced in Figure 2. We have found that if the shell is placed at some distance from the core, then it is difficult to reproduce the observations as almost all lines appear in emission within the LWS beam ( $80''$ ). Even if the shell is contiguous to the core but large in thickness, lines also appear in emission. Models in Fig. 2 correspond to a total size of  $42''$  ( $5.3 \times 10^{18} \text{ cm}$ ) for the core+shell cloud.

The model labelled  $M_1$  corresponds to  $T_K=40 \text{ K}$ ,  $n(\text{H}_2)=10^4 \text{ cm}^{-3}$  and  $\chi(\text{OH}) = 2 \times 10^{-6}$ . The cross-ladder and  $^2\Pi_{3/2}$  transitions are in absorption while the  $^2\Pi_{1/2}$  intra-ladder transitions are predicted in emission. However, although the intensity of the absorbing lines is found to fit reasonably well the observations, emission lines are underestimated. If the OH abundance is increased in order to reproduce the intensity of the emitting lines then, absorbing lines are poorly fitted as limb effects start to dominate. This effect is already seen in the  $J=1/2 \leftarrow 3/2$  cross-ladder transition at  $\sim 79 \mu\text{m}$ . In particular, the  $^2\Pi_{1/2} J=5/2 \rightarrow 3/2$  transition at  $\sim 98 \mu\text{m}$  is strongly underestimated by model  $M_1$ . If the gas temperature increases, collisions start to pump the OH levels and the intensity of the  $\sim 98 \mu\text{m}$  line is better fitted. However, a new problem arises as strong asymmetries in the line intensities of each  $\Lambda$ -doubling line do appear at high temperature (no asymmetries have been observed within the S/N ratio of the data). These asymmetries were already predicted by OfD and are due to a strong parity change propensity rule introduced by collisions with para- $\text{H}_2$ . They can only be suppressed if the  $\text{H}_2$  ortho-to-para (OTP) ratio is higher or if radiative

pumping dominates. We have adopted a OTP ratio of 3. Model M<sub>2</sub> in Fig. 2 corresponds to T<sub>K</sub>=150 K with otherwise the same parameters as M<sub>1</sub>. The intensity of the  $\sim 98 \mu\text{m}$  doublet is considerably enhanced with respect to the low temperature model. The intensity asymmetry in this doublet is not visible in the data as the doublet is unresolved with the LWS/FP spectrometer. The effect of the IR pumping strongly reduces the asymmetries that could be present without the optically thick core. Finally, model M<sub>3</sub> (thick lines in Figure 2) represents T<sub>K</sub>=300 K,  $n(\text{H}_2)=5\times 10^3 \text{ cm}^{-3}$  and  $\chi(\text{OH}) = 3 \times 10^{-6}$ . Again, the strong asymmetry of the  $\sim 98 \mu\text{m}$  doublet is not observable due to the lack of spectral resolution. However, the observed total intensity for the doublet agrees well with that predicted from the model. For the other lines, M<sub>3</sub> reproduces qualitatively well the observed OH pattern, except in the line wings in the 119 and 79  $\mu\text{m}$  doublets. Nevertheless, cold foreground gas (not included in the model) absorbs (like in M<sub>1</sub>) at these wavelengths, reducing the emission wing effects in these lines.

From our models it is clear that the gas surrounding Sgr B2 has to be warm (see Ceccarelli et al. 2002) and must have a moderate H<sub>2</sub> density. The OH abundance is rather high,  $(2-5)\times 10^{-6}$ . Assuming that M<sub>3</sub> represents a reasonable fit to the OH data, we derive  $N(^{18}\text{OH})=(6\pm 2)\times 10^{13} \text{ cm}^{-2}$  for Sgr B2. Hence, the  $^{16}\text{O}/^{18}\text{O}$  isotopic ratio is 240–280, in excellent agreement with the value obtained by Bujarrabal, Cernicharo & Guélin (1983) from the OH 18 cm lines and a factor  $\simeq 2$  lower than in the  $V_{\text{LSR}} \simeq 0 \text{ km s}^{-1}$  component. Higher T<sub>K</sub> could even be possible but the actual collisional rates introduce very strong intensity asymmetries in the cross-ladder transitions which are not observed. If the gas temperature is higher, then its density has to be lower than the value used in M<sub>3</sub> ( $5\times 10^3 \text{ cm}^{-3}$ ). The reason is that higher temperatures produce strong emission in the OH high excitation transitions ( $\sim 71$  and  $\sim 65 \mu\text{m}$  for example, see Figure 2) which is not observed. For T<sub>K</sub>=600 K,  $n(\text{H}_2)$  has to be decreased to  $(1-2)\times 10^3 \text{ cm}^{-3}$  and  $\chi(\text{OH})$  increased to  $(0.5-1)\times 10^{-5}$  to obtain a crude fit the ISO data. A temperature gradient across the shell, going from T<sub>K</sub>=40 K in the innermost regions to T<sub>K</sub>=600 K in the external layers is probably a better representation to the physical structure of the edge of the Sgr B2 cloud.

The inferred  $^{16}\text{OH}$  column density in the shell,  $(1.5-2.5)\times 10^{16} \text{ cm}^{-2}$ , and that of H<sub>2</sub><sup>16</sup>O determined also from LWS/FP data (Cernicharo et al. 1997; 2002, in preparation) leads to an OH/H<sub>2</sub>O=0.1–1 abundance ratio. For comparison, shock models of Flower et al. predict  $\simeq 10^{-3}$ , while models of dense dark cores predict  $\simeq 10^{-4}$ . On the other hand, the maximum OH abundance in PDR models is  $\simeq 10^{-5}$  with OH/H<sub>2</sub>O ratios close to 10. The large abundance found in Sgr B2 suggests that its external shells are illuminated by a strong UV field producing a PDR, although low velocity shocks ( $v_S \sim 30 \text{ km s}^{-1}$ ), unresolved by the ISO data, may be also present. Many species formed during the evolution of the cold gas in Sgr B2 are being now reprocessed in these regions. This warm gas is poorly traced

by millimeter and submillimeter observations, but it represents the strongest contribution to the absorption/emission features in the far-IR spectrum of Sgr B2. In addition to  $^{16}\text{OH}$  and  $^{18}\text{OH}$ , we have searched for several related species such as  $\text{OH}^+$  or  $\text{H}_2\text{O}^+$ . No lines from these species have been found.

The future far-IR instruments on board next generation telescopes such as the *Herschel Space Observatory* will allow a fast mapping of many OH rotational lines in galactic and extragalactic sources making OH a very useful tool in deriving the physical properties of GC giant molecular clouds. This could help in the analysis of starburst galaxies like Arp 220.

We thank Spanish DGES and PNIE for funding support under grant ESP98-1351-E and PANAYA2000-1784 and C.M. Walmsley, V. Bujarrabal and J. Fischer for their comments on the manuscript. We also thank our referee, E.F. van Dishoeck, for her useful comments and suggestions. JRG acknowledges *UAM* for a pre-doctoral fellowship.

## REFERENCES

- Bergin, E.A., Langer, W.D., Goldsmith, P.F. 1995 ApJ, 441, 222
- Betz, A.L., & Boreiko, R.T. 1989, ApJ, 346, L101
- Bujarrabal, V., Cernicharo, J., & Guelin, M. 1983, A&A, 128, 355
- Ceccarelli, C. et al. 2002, A&A, 383, 603
- Cernicharo, J., Lim, T., Cox, P., et al. 1997, A&A, 323, L25
- Cernicharo, J., Orlandi, M.A., González-Alfonso, E., & Leeks, S.J. 1999, in “The Universe as seen by ISO”, Eds. P. Cox & M.F. Kessler, ESA-SP 427, 655
- Clegg, P.E., et al. 1996, A&A, 315, L38
- Cox, P., & Laureijs, R. 1989, in “The Center of the Galaxy”, Ed. Morris, M., IAU, Sym.No. 136, 121
- de Graauw, T. et al. 1996, 315, L49
- Draine, B.T., Roberge, W.G., & Dalgarno, A. 1983, ApJ, 264, 485
- Flower, D.R., Pineau des Forêts & M.C. Walmsley, 1995, 294, 815
- Goicoechea, J.R., & Cernicharo, J. 2001, ApJ, 554, L213
- Goldsmith, P.F., Lis, D.C., Lester, D.F., & Harvey, P.M. 1992, ApJ, 389, 338
- González-Alfonso E., Cernicharo J., 1993, A.&A., 279, 506
- Greaves, J.S. & Williams, P.G. 1994, A&A, 290, 259
- Greaves, J.S. 1995, MNRAS, 273, 918
- Kessler, M.F., et al. 1996, A&A, 315, L27
- Lis, D.C., & Goldsmith, P.F. 1989, ApJ, 337, 704
- Martín-Pintado, J., Gaume, R.A., Rodríguez-Fernández, N., de Vicente, P., & Wilson, T.L. 1999, ApJ, 519, 667
- Melnick, G.J., Genzel, R., & Lugten, J.B. 1987, ApJ, 321, 530
- Melnick, G.J., Stacey, G.J., Genzel, R., Lugten, J.B. & Poglitsch, A. 1990, ApJ, 348, 161



- Neufeld, D.A., Lepp, S., & Melnick, G.J. 1995, ApJS, 100, 132
- Neufeld, D.A., et al. 2000, ApJ, 539, L111
- Offer, A.R., & van Dishoeck, E.F. 1992, MNRAS, 257, 377 (OfD)
- Offer, A.R., van Hemert, M.C., & van Dishoeck, E.F. 1994, JChPh, 100, 362 (OfHD)
- Pierce–Price, D., Richer, J.S., Greaves, J.S. et al. 2000, ApJ, 545, L121
- Scoville, N.Z. 1972, ApJ, 175, L127
- Scoville, N.Z., Solomon, P.M. & Penzias, A.A. 1975, ApJ, 201, 352
- Sternberg, A., & Dalgarno, A. 1995, ApJS, 99, 565
- Storey, J., Watson, D.M., & Townes, C.H. 1981, ApJ, 244, L27
- Swinyard, B.M., et al. 1998, SPIE, 3354, 888
- Van Dishoeck, E.F., & Black, J.H. 1986, ApJS, 62, 109
- Vicuso, P.J., et al. 1985, ApJ, 296, 149
- Watson, D.M., Genzel, R., Townes, C.H., & Storey, J.W.V. 1985, ApJ, 298, 316

Fig. 1.— ISO observations of  $^{16}\text{OH}$  and  $^{18}\text{OH}$  toward Sgr B2 M and rotational energy diagram of OH. The two ladders,  $^2\Pi_{3/2}$  and  $^2\Pi_{1/2}$ , produced by the spin orbit interaction are shown. The  $\Lambda$ -doubling splitting of each rotational level has been enhanced for clarity. The hyperfine structure of the rotational levels is not shown. The observed rotational transitions are indicated by arrows and the observed ISO line profiles are shown in boxes. The intensity scale corresponds to the continuum normalized flux and the abscissa to the wavelength in microns. When lines are centered only at Sgr B2 velocities ( $\simeq +50 \text{ km s}^{-1}$ ), the LSR velocity scale is not shown. All  $\Lambda$ -doublets are LWS/FP data excepting the  $34.6 \mu\text{m}$  doublet for which SWS grating data ( $\lambda/\Delta\lambda \simeq 1500$ ) are shown. One component has been observed with the SWS/FP ( $\lambda/\Delta\lambda \simeq 30000$ ) and data are shown in the inset of the corresponding box. The  $^{18}\text{OH } ^2\Pi_{3/2} \text{ J}=5/2 \leftarrow 3/2$  doublet is shown in the upper inset.

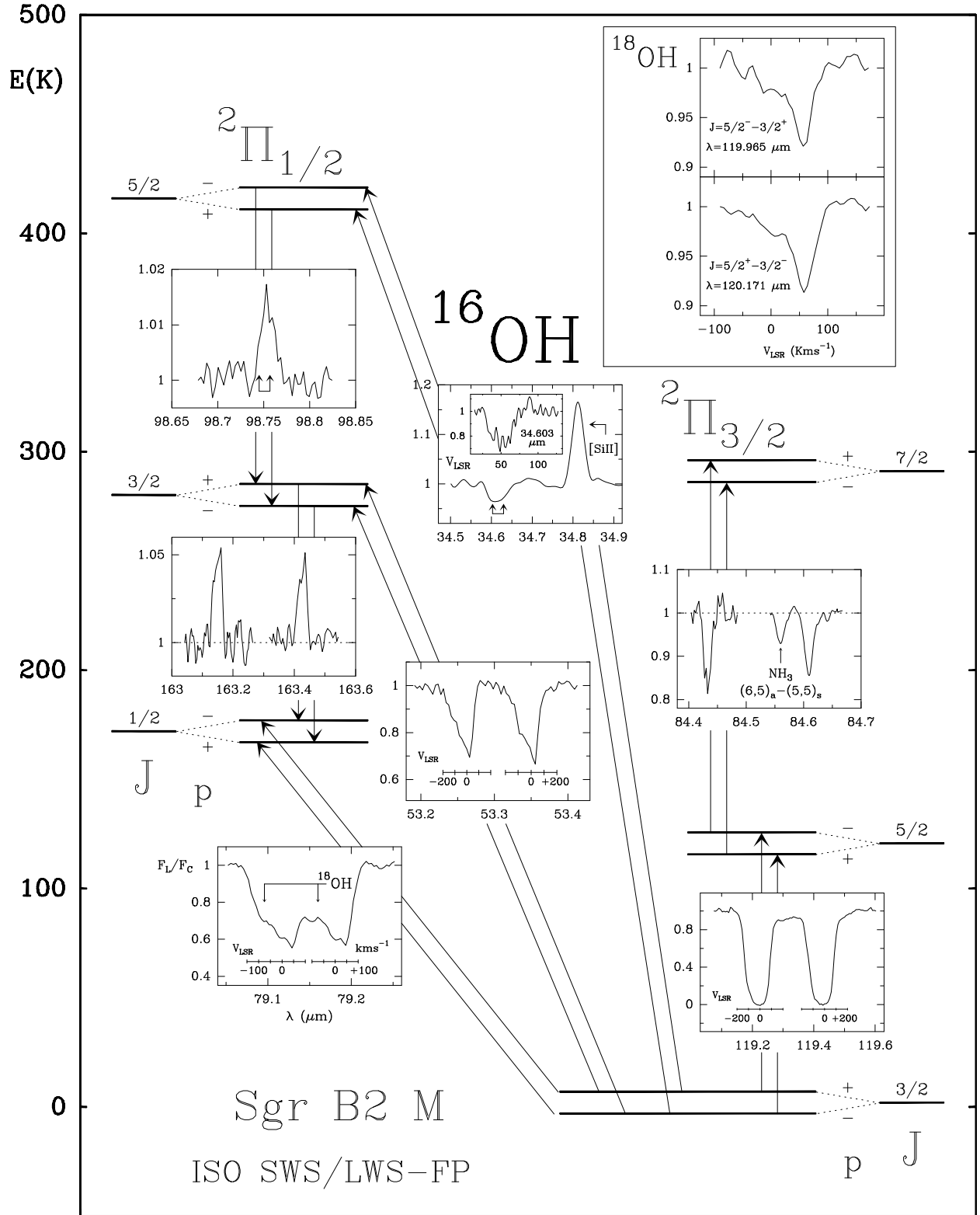


Fig. 2.— Results from selected models of Sgr B2 component ( $V_{LSR} \simeq +50 \text{ km s}^{-1}$ ) discussed in the text. The central panels correspond to the cross-ladder transitions of OH. Line intensities have been normalized to the continuum dust emission. The wavelength of the transitions is indicated at the right of each panel. The model labelled M<sub>1</sub> corresponds to  $T_k=40 \text{ K}$ ,  $n(\text{H}_2)=10^4 \text{ cm}^{-2}$ ,  $\chi_{OH}=2 \times 10^{-6}$ . The model labelled M<sub>2</sub> corresponds to  $T_k=150 \text{ K}$ ,  $n(\text{H}_2)=10^4 \text{ cm}^{-2}$ ,  $\chi_{OH}=2 \times 10^{-6}$ . The model labelled M<sub>3</sub> corresponds to  $T_k=300 \text{ K}$ ,  $n(\text{H}_2)=5 \times 10^3 \text{ cm}^{-2}$ ,  $\chi_{OH}=3 \times 10^{-6}$ . The velocity resolution in the modeled line profiles is  $1 \text{ km s}^{-1}$ .

